Supplemental Material

Mechanistic links between Na^+ channel (SCN5A) mutations and impaired cardiac pacemaking in sick sinus syndrome

*Timothy D. Butters[1], *Oleg V. Aslanidi[1], Shin Inada[2], Mark R. Boyett[2], Jules C. Hancox[3], Ming Lei[2], Henggui Zhang[1]

[1]*Biological Physics Group, School of Physics and Astronomy, University of Manchester, Manchester M13 9PL, United Kingdom*

[2]*Cardiovascular Research Group, Faculty of Medical and Human Sciences, University of Manchester, Manchester M13 9NT, United Kingdom*

[3]*Department of Physiology and Pharmacology, Cardiovascular Research Laboratories, Bristol Heart Institute, School of Medical Sciences, University of Bristol, Bristol BS8 1TD, United Kingdom*

*Joint first authors

METHODS

2D slice model

The dynamics of initiation and conduction of electrical APs in the heart can be modelled using the standard Hodgkin-Huxley-type partial differential equation:[1,2]

$$\frac{\partial V}{\partial t} = \nabla \cdot (D \nabla V) - \frac{I_{\text{tot}}}{C_m}, \quad (1)$$

where V is the membrane potential, t time, ∇ the spatial gradient operator, D the diffusion coefficient that characterises electrotonic spread of voltage via gap junctions, C_{m} the cell membrane capacitance and I_{tot} the total ionic current. Electrophysiologically-detailed models for I_{tot} – and hence, single cell APs – have been developed for rabbit SAN[1] and RA[2] cells.

The 2D model of intact SAN-atrium tissue was based on histologically reconstructed[3] geometry of a single slice of the rabbit RA, which was cut through the atrial muscle of the crista terminalis and the intercaval region with central and peripheral SAN areas (Fig. 1A). The geometry presents a high spatial resolution (40 μm, which corresponds to 2 to 4 diameters of a cardiac myocyte) regular Cartesian grid of 210 × 45 nodes. For each node, a flag variable was used to identify whether it belongs to the SAN or RA cell type based on immunohistochemistry mapping data.[3] The SAN was modelled by the Zhang *et al*. equations[1] for central and peripheral cells, and the RA was modelled by the Aslanidi *et al*. equations[2] for atrial cells, with each model producing different AP morphology (Fig. 1A).

The 2D model also incorporated an experimentally observed non-conductive region ("block zone") next to the SAN towards the atrial septum, where cells have low excitability. In the block zone, I_{tot} in Equation 1 was described as:

$$I_{\text{tot}} \equiv I_{\text{B}} = G_{\text{m}}(V - V_{\text{R}}). \quad (2)$$

Here I_{B} is the passive membrane current, G_{m} is the membrane conductance, and V_{R} the resting membrane potential. Values for G_{m} and V_{R} were assumed to correspond to the membrane conductance and resting potential of the surrounding atrial tissue.

The AP conduction in the 2D tissue model due to intercellular electrical coupling via gap junctions was modelled through the diffusion coefficient, D. In the model, we considered the regional differences in the electrophysiological properties and gap junctional coupling between the SAN centre, periphery and atrial tissue as observed experimentally.[3] A spatial gradient of D (Fig. 1F) was introduced as in our previous study:[4]

$$D(x) = D_c + D_p\left(\frac{1.0}{1.0+e^{-0.5(x-x_1)}} + \frac{1.0}{1.0+e^{0.5(x-x_2)}}\right), \quad (3)$$

where x is the horizontal coordinate through the 2D slice, x_1 and x_2 approximately correspond to the positions of the SAN boundaries within the tissue, and D_c and D_p are the diffusion coefficients of central and peripheral SAN cells, respectively.

The 2D model also considered the regional differences in the cellular electrical properties of SAN cells. The gradient distributions of current densities from the central to the peripheral SAN were modelled by correlating them to cell membrane capacitance (C_m), which was assumed to be small in the centre and large in the periphery.[1,4] The spatial gradient distribution of C_m (Fig. 1E) was modelled as:

$$C_m(x) = C_m^c + C_m^p\left(\frac{1.0}{1.0+e^{-0.1(x-x_1)}} + \frac{1.0}{1.0+e^{0.1(x-x_2)}}\right), \quad (4)$$

where C_m^c and C_m^p are the capacitances of central and peripheral SAN cells, respectively.

Spatial variations in all ion channel conductances were defined as a function of C_m as found experimentally:[1]

$$g_Z(x) = \frac{C_m(x)-C_m^c}{C_m^p-C_m^c}\,g_Z^c + \frac{C_m^p-C_m(x)}{C_m^p-C_m^c}\,g_Z^p \quad , \quad (5)$$

where $g_Z(x)$ is the conductance of one of the currents $Z \in \{Na, Ca, K, \ldots\}$, and g_Z^c and g_Z^p are the respective conductances for central and peripheral SAN cells.

ACh effects

ACh decreases the heart rate by slowing down the spontaneous diastolic depolarization rate of the SAN. In order to incorporate the effects of ACh into the cell models, an ACh-activated K^+ current, $I_{K,ACh}$, was introduced as part of I_{tot}:[5]

$$I_{K,ACh} = g_{K,ACh}\left(\frac{[K^+]_o}{10+[K^+]_o}\right)\cdot\left(\frac{V-E_K}{1+e^{(V-E_K-140)F/2.5RT}}\right), \quad (6)$$

where $g_{K,ACh}$ is the maximum channel conductance, $[K^+]_o$ is the extracellular K^+ concentration, E_K is the equilibrium potential for K^+ and F, R and T have their usual meanings. The conductance, $g_{K,ACh}$, is ACh dose-dependent, as follows:

$$g_{\mathrm{K,ACh}} = g_{\mathrm{K,ACh,max}}\, jk \frac{[\mathrm{ACh}]^{n\mathrm{K,ACh}}}{K_{0.5,\mathrm{K,ACh}}^{n\mathrm{K,ACh}} + [\mathrm{ACh}]^{n\mathrm{K,ACh}}}, \quad (7)$$

where $g_{\mathrm{K,ACh,max}}$ is the maximum value of $g_{\mathrm{K,ACh}}$, j and k are inactivation variables, [ACh] is the ACh concentration, $n_{\mathrm{K,ACh}}$ is the Hill coefficient, and $K_{0.5,\mathrm{K,ACh}}$ is the ACh concentration that produces half-maximal activation of $g_{\mathrm{K,ACh}}$. $I_{\mathrm{K,ACh}}$ is included in both the SAN and atrial cell models, with $g_{\mathrm{K,ACh,max}}$ described by the same spatial gradient function as the other ion channel conductances, see Equation 5.

ACh also partially inhibits the L-type Ca^{2+} current, $I_{\mathrm{Ca,L}}$, and shifts the activation curve of the hyperpolarization-activated current, I_{f}, towards more negative potentials. The fractional block, b, for $I_{\mathrm{Ca,L}}$ is given by:[5]

$$b = b_{\max} \frac{[\mathrm{ACh}]}{K_{0.5,\mathrm{Ca}} + [\mathrm{ACh}]}, \quad (8)$$

where $b_{\max}$ is the maximum fraction of $I_{\mathrm{Ca,L}}$ block, and $K_{0.5,\mathrm{Ca}}$ is the ACh concentration that produces a half maximal block of $I_{\mathrm{Ca,L}}$. The shift in I_{f} activation curve is given by:[5]

$$s = s_{\max} \frac{[\mathrm{ACh}]^{n\mathrm{f}}}{K_{0.5,\mathrm{f}}^{n\mathrm{f}} + [\mathrm{ACh}]^{n\mathrm{f}}}, \quad (9)$$

where $s_{\max}$ is the maximum shift of the I_{f} activation curve, n_{f} is the Hill coefficient, and $K_{0.5,\mathrm{f}}$ is the ACh concentration that produces a half maximal shift of the activation curve of I_{f}.

SCN5A mutation model

In order to model SCN5A mutations from G1 (T220I, P1298L and delF1617), parameters of the fast Na^+ current, I_{Na}, were changed to reproduce experimental data (see in Fig. 2). Note that prior experimental data[6] were recorded from tsA201 cells transfected with a recombinant human Na^+ channel cDNA (hH1), whereas our models are for the native current in rabbit SAN cells. In simulations, we shifted the steady-state inactivation curve by the same amount as observed experimentally (Figs. 2C and 2D) and implemented the same percentage changes of the fast- and slow-inactivation time constants as observed experimentally (Fig. 2A). We scaled the maximal I_{Na} channel conductance by a factor S_{CD} to reproduce the normalised I-V relationship (Fig. 2E) and the reduction in I_{Na} as observed experimentally (Fig. 2F).

For a mutant model, the I_{Na} equation becomes:

$$I_{\mathrm{Na}} = \left(S_{\mathrm{CD}} \times g_{\mathrm{Na}}\right) m^3 h [\mathrm{Na}^+]_{\mathrm{o}} \frac{F^2}{RT} \frac{e^{(V - E_{\mathrm{Na}})F/RT} - 1}{e^{VF/RT} - 1} V, \quad (10)$$

with inactivation time constants:

$$\tau_{h_1} = S_{\tau_{h1}}\left(\frac{3.717\times10^{-6}e^{-0.2815(V+17.11)}}{1+3.732\times10^{-3}e^{-0.3426(V+37.76)}}+5.977\times10^{-4}\right), \quad (11)$$

$$\tau_{h_2} = S_{\tau_{h2}}\left(\frac{3.186\times10^{-8}e^{-0.6219(V+18.8)}}{1+7.189\times10^{-5}e^{-0.6683(V+34.07)}}+3.556\times10^{-3}\right), \quad (12)$$

and voltage-dependent steady-state inactivation function, $h_{1\infty}$:

$$h_{1\infty} = \frac{1}{1+e^{\left(V-V*S_h+66.1\right)/6.4}}, \quad (13)$$

where $V*S_h$ (mV) is a shift in the inactivation curve.

The heterozygous E161K mutation was modelled by the same method as used by Smits *et al.*[7] I_{Na} was divided into two components – one for the WT I_{Na} and another for the E161K mutant I_{Na}. The WT component had a maximum conductance of 50% of control, whereas the mutant component had a maximum conductance of 20% of control. The steady-state activation curve of the mutant component was also shifted by 11.9 mV (see in Fig. 2B):

$$m_{\infty}^3 = \frac{1}{1+e^{-(V-11.9)/5.46}}. \quad (14)$$

A full list of the model equations and parameters used for the SAN central and peripheral cells and RA cells is presented below (Models I-III and Tables I-III).

Numerical algorithms

The 2D anatomical PDE model of the intact SAN-atrium was solved using the explicit Euler method with a 5-node approximation of the Laplacian operator. In numerical simulations, the time step was 0.005 ms and space step 0.04 mm, which gave accurate numerical solutions.

Safety factor

Safety factor (SF) has been introduced as a simple index of the robustness of conduction in cardiac tissues: it is defined as the ratio of charge generated to charge consumed by a cell during its excitation.[8] $SF > 1$ indicates successful conduction, with the fraction of the value exceeding 1 indicative of the margin of safety. When SF is close to 1, conduction is critical, and when $SF < 1$, propagation fails. The equation used to compute SF is:

$$\mathrm{SF} = \frac{\int_A I_c \mathrm{d}t + \int_A I_{out} \mathrm{d}t}{\int_A I_{in} \mathrm{d}t}; A \mid t \in [t_{1\%}, t_{V_{max}}] \quad (15)$$

Here, I_c is the capacitive current of the cell, I_{out} is the intercellular current that flows from the cell to its downstream neighbour and I_{in} is the intercellular current that flows into the cell from its upstream neighbour. The domain of integration, *A*, can be defined as the period of time from the moment when $\mathrm{d}V/\mathrm{d}t$ at the AP wavefront reaches 1% of its maximum to the moment when V reaches its maximum.[9]

Isolated tissue experiments

5 male adult rabbits (2-3 months old) were used for experimental study. The sino-atrial preparations were set up as described previously from animals killed by anesthetic overdose with venous injection of sodium phenobarbital (in accord with UK Home Office Legislation).[10] After excision of the SAN and surrounding atrial muscle, the preparation was placed endocardial surface upwards in a tissue bath and superfused with modified Tyrode's solution (in mmol/L: NaCl 120, $NaHCO_3$ 25.2, NaH_2PO4 1.2, $MgCl_2$ 1.3, glucose 5, KCl 4.0, $CaCl_2$ 1.8, gassed with 95% O_2/5% CO_2) at 37 °C and at a flow rate of ~5 ml/min. Electrical signals were obtained from the surface of this preparation by apposition of a custom-made extracellular multi-electrode array that allowed electrograms to be monitored at multiple sites in the tissue as excitation passed under the array. The electrode array held 30 separate silver electrodes in a 5×6 configuration. The inter-electrode distance was 0.55 mm; thus, the total array dimensions were approximately 3 mm length and 4 mm width. The electrodes were Teflon-coated silver wires with a coated outer diameter of 0.2 mm and an inner diameter of 0.125 mm (Science Products, Millville, NJ, USA). The spacing of the electrodes was obtained with 0.33 Teflon coated silver wires. The silver tips were chlorided. The 30 recording electrodes were connected through shielded wires to a 32-channel amplifier (SCXI-1102C, National Instruments Corporation UK Ltd, Newbury, UK). The sampling frequency for each channel was set at 1 kHz. The signals were continuously sampled and stored on disk and displayed on screen using a custom-developed program, written in Labview 7.0 (National Instruments Corporation UK Ltd, Newbury, Berks RG14 2PS, UK). Experiments were performed under the conditions of control, application of tetrodotoxin (TTX) (0.5 μmol/L; IC_{50} ~ 0.1 μmol/L) or a non-degrading ACh equivalent – carbachol (CCh) (200 nmol/L; IC_{50} ~ 100 nmol/L), and a combination of TTX (0.5 μmol/L) and CCh (200 nmol/L). Propagation

maps were then derived during off-line analysis. The signals were displayed on screen in sets of 8 to 16 electrograms. The activation time was denoted as the point of maximal negative slope and marked with a cursor. After marking all significant waveforms in all leads, the activation times were then displayed in a grid representing the layout of the original recording array. All activation times, in milliseconds, were related to the timing of the first detected waveform. Areas of isochronal activation in steps of 5 ms were plotted using the standard visualization package Paraview 6.0.

RESULTS

Effects on excitability

The G1 and G2 groups of SCN5A mutations modulate atrial excitability differently: one through shifting the steady-state inactivation curve to more negative potentials with the other shifting the steady-state activation curve to more positive potentials. Therefore, a systematic analysis of effects of activation and inactivation shifts on excitability and conduction was undertaken, the results of which are shown in Online Fig. I. Online Fig. IA, B shows plots of conduction velocity in a 1D strand of atrial cells against a range of inactivation shifts towards more negative potentials (Online Fig. IA), and a range of activation shifts towards more positive potentials (Online Fig. IB). In both cases, with the increase of the shift (0 corresponds to the WT channel), the measured conduction velocity monotonically decreased until conduction failed. This occurred at a -14 mV shift in inactivation $V_{0.5}$ and a 7 mV shift in activation $V_{0.5}$. Such a difference in the 'cut-off' shift values for these two cases can be explained by differential change of the excitation threshold; this is shown in Online Fig. IC, D. These panels show plots of excitation threshold (measured as the minimal amplitude of an external current stimulus that provokes an atrial action potential) against a shift in steady-state inactivation (Online Fig. IC) or activation (Online Fig. ID). In both cases, a linear increase in the shift resulted in a monotonic increase in the measured excitation threshold. However, with the same value, the G2 shift always increased more the measured excitation threshold than the G1 shift (compare Online Figs. ID and IC). For the G1 case (Online Fig. IC), the excitation threshold increased from ~1.55 nA with the WT channel to ~1.65 nA when the inactivation curve was shifted by -14 mV; for the G2 case (Online Fig. ID), the threshold increased from ~1.55 nA with the WT channel to ~2 nA when the activation curve was shifted by +7 mV – for larger shift values the threshold kept increasing, and although APs could still be initiated

in a single cell, their conduction in the tissue failed. Simulated addition of 1.5×10^{-8} mol/L ACh enhanced the effects described above, further decreasing the conduction velocities (Online Figs. IA and IB) and increasing the excitation thresholds (Online Figs. IC and ID) for both G1 and G2 mutations. This combination of effects can account for the higher susceptibility to conduction block in the 2D mutant tissues with ACh (see Fig. 6).

Effects on conduction safety

We further studied the effects of the SCN5A mutations and ACh on SF in the 2D model of SAN-atrium tissue. Online Fig. II illustrates SF distributions in the 2D tissue during AP conduction from the SAN into the RA. For the WT condition, SF was greater than 1 in all regions of the tissue, indicating safe conduction. Note that slightly smaller values of SF in the crista terminalis, as compared to the rest of the RA, were due to higher source-to-load mismatch within this thick bundle (large integral I_{in} flowing from the SAN, relatively small integral I_{out} flowing out to the RA). SCN5A Na^+ channel mutations for both the G1 (P1298L) and G2 (E161K) groups resulted in decreases throughout the tissue in the AP conduction velocity, dV/dt_{max} (see in Fig. 7) and SF (Online Fig. II), all of which were decreased greater in the G2 (E161K) group than in the G1 (P1298L) group. Simulated addition of 1.5×10^{-8} mol/L ACh reduced SF in both WT and mutant cases. Again, reduction in SF was relatively greater in the G2 (E161K) mutation condition – in the region close to the exit-site from the crista terminalis into the RA, SF became less than 1 (Online Fig. II) leading to a conduction block in this direction (see in Fig. 6). Note that an apparent localised increase of SF within the crista terminalis in case of the E161K mutation was due to a large decrease of the AP conduction velocity (see in Fig. 7) – such a decrease allowed a time delay sufficient to balance out the source-to-load mismatch[9] within this region. However, even though a source-to-load mismatch close to a narrow exit site from the crista terminalis towards the RA was similarly reduced, a substantial decrease of dV/dt_{max} in this region due to the combination of the E161K mutation and ACh (Fig. 7) resulted in a large decrease of the capacitive current $I_c = C_m dV/dt$ – leading to a large decrease of SF and the resultant AP conduction block in this direction (see in Fig. 6 and Online Fig. II). The results of these simulations suggest that (i) the G2 (E161K) mutation results in the largest decrease of SF due to the largest decreases of dV/dt_{max} and the AP conduction velocity as compared to the G1 SCN5A mutations (Figs. 7 and Online Fig. II); (ii) the AP conduction block due to the combination of the E161K mutation and high ACh concentration emerges from a decrease of SF localized close to the

exit-site from the crista terminalis towards the RA (Online Fig. II), where both the source-to-load mismatch due to narrowing of the RA tissue and the reduction of dV/dt_{max} are substantial.

References

1. Zhang H, Holden AV, Kodama I, Honjo H, Lei M, Varghese T et al. Mathematical models of action potentials in the periphery and center of the rabbit sinoatrial node. *Am J Physiol Heart Circ Physiol.* 2000;279:397-421.
2. Aslanidi OV, Boyett MR, Dobrzynski H, Li J, Zhang H. Mechanisms of transition from normal to reentrant electrical activity in a model of rabbit atrial tissue: interaction of tissue heterogeneity and anisotropy. *Biophys J.* 2009;96:798-817.
3. Dobrzynski H, Li J, Tellez J, Greener ID, Nikolski VP, Wright SE et al. Computer three-dimensional reconstruction of the sinoatrial node. *Circulation*. 2005;111:846-854.
4. Zhang H, Zhao Y, Lei M, Dobrzynski H, Liu JH, Holden AV *et al.* Computational evaluation of the roles of Na^+ current, i_{Na}, and cell death in cardiac pacemaking and driving. *Am J Physiol Heart Circ Physiol.* 2007;292:H165-H174.
5. Zhang H, Holden AV, Noble D, Boyett MR. Analysis of the chronotropic effect of acetylcholine on sinoatrial node cells. *J Cardiovasc Electrophysiol.* 2002;13:465-474.
6. Benson DW, Wang DW, Dyment M, Knilans TK, Fish FA, Strieper MJ *et al*. Congenital sick sinus syndrome caused by recessive mutations in the cardiac sodium channel gene (SCN5A). *J Clin Invest.* 2003;112:1019-1028.
7. Smits JP, Koopmann TT, Wilders R, Veldkamp MW, Opthof T *et al*. A mutation in the human cardiac sodium channel (E161K) contributes to sick sinus syndrome, conduction disease and Brugada syndrome in two families. *J Mol Cell Cardiol.* 2005;38:969-981.
8. Shaw RM, Rudy Y. Ionic mechanisms of propagation in cardiac tissue: roles of the sodium and L-type calcium currents during reduced excitability and decreased gap junction coupling. *Circ Res.* 1997;81:727-741.
9. Aslanidi OV, Stewart P, Boyett MR, Zhang H. Optimal velocity and safety of discontinuous conduction through the heterogeneous Purkinje-ventricular junction. *Biophys J.* 2009;97:20-39.
10. Lei M, Jones SA, Liu J, Lancaster MK, Fung SS-M, Dobrzynski H, Camelliti P, Maier SKG, Noble D, Boyett MR. Requirement of neuronal- and cardiac-type sodium channels for murine sinoatrial node pacemaking. *J Physiol (Lond.)* 2004;559:835-848.

Online Table I. Values for mutation parameters.

Mutation	S_{CD}	S_h	$S_{\tau_{h_1}}$	$S_{\tau_{h_2}}$
T220I	0.62	0.049	2.51	3.28
P1298L	0.45	0.138	2.91	4.79
DelF1617	0.38	0.128	2.18	2.75

Model I. General single cell equations

$$\frac{\mathrm{d}V}{\mathrm{d}t} = -\frac{I_{\mathrm{tot}}}{C_m}$$

Model I.1. Equilibrium potentials

$$E_{\mathrm{Na}} = \frac{RT}{F}\ln\frac{[\mathrm{Na}^+]_{\mathrm{o}}}{[\mathrm{Na}^+]_{\mathrm{i}}}, \quad E_{\mathrm{K}} = \frac{RT}{F}\ln\frac{[\mathrm{K}^+]_{\mathrm{o}}}{[\mathrm{K}^+]_{\mathrm{i}}}, \quad E_{\mathrm{Ca}} = \frac{RT}{2F}\ln\frac{[\mathrm{Ca}^{2+}]_{\mathrm{o}}}{[\mathrm{Ca}^{2+}]_{\mathrm{i}}}, \quad E_{\mathrm{Cl}} = \frac{RT}{F}\ln\frac{[\mathrm{Cl}^-]_{\mathrm{o}}}{[\mathrm{Ca}^-]_{\mathrm{i}}}$$

Model II. SAN cell model

$$I_{\mathrm{tot}} = I_{\mathrm{Na}} + I_{\mathrm{Ca,L}} + I_{\mathrm{Ca,T}} + I_{\mathrm{to}} + I_{\mathrm{sus}} + I_{\mathrm{K,r}} + I_{\mathrm{K,s}} + I_f + I_{K,b} + I_{\mathrm{Na,b}} + I_{\mathrm{Ca,b}} + I_{\mathrm{NaCa}} + I_{\mathrm{NaK}} + I_{ACh}$$

Model II.1. Fast Na^+ current

$$I_{\mathrm{Na}} = g_{\mathrm{Na}} m^3 h [\mathrm{Na}^+]_{\mathrm{o}} \frac{VF^2}{RT}\frac{e^{(V-E_{\mathrm{Na}})F/RT}-1}{e^{VF/RT}-1}$$

$$\frac{\mathrm{d}m}{\mathrm{d}t} = \frac{m_\infty - m}{\tau_m}$$

$$m_\infty = \left(\frac{1}{1+e^{-V/5.46}}\right)^{1/3}, \quad \tau_m = 1000\left(\frac{0.6247\times10^{-2}}{0.832\, e^{-0.335\,(V+56.7)} + 0.627\, e^{0.082\,(V+65.01)}} + 4\times10^{-5}\right)$$

$$h = (1-F_{Na})h_1 + F_{Na}h_2, \quad F_{Na} = \frac{9.52\times10^{-2}\, e^{-6.3\times10^{-2}(V+34.4)}}{1+1.66\, e^{-0.225\,(V+63.7)}} + 8.69\times10^{-2}$$

$$\frac{\mathrm{d}h_1}{\mathrm{d}t} = \frac{h_{1\infty}-h_1}{\tau_{h_1}}, \quad \frac{\mathrm{d}h_2}{\mathrm{d}t} = \frac{h_{2\infty}-h_2}{\tau_{h_2}}$$

$$h_{1\infty} = h_{2\infty} = \frac{1}{1+e^{(V+66.1)/6.4}}$$

$$\tau_{h_1} = 1000\left(\frac{3.717\times10^{-6}\, e^{-0.2815\,(V+17.11)}}{1+3.732\times10^{-3}\, e^{-0.3426\,(V+37.76)}} + 5.977\times10^{-4}\right)$$

$$\tau_{h_2} = 1000\left(\frac{3.186\times10^{-8}\, e^{-0.6219\,(V+18.8)}}{1+7.189\times10^{-5}\, e^{-0.6683\,(V+34.07)}} + 3.556\times10\right)$$

Model II.2. L-type Ca^{2+} current

$$I_{\mathrm{Ca,L}} = g_{\mathrm{Ca,L}}\left(d_{\mathrm{L}} f_{\mathrm{L}} + \frac{0.006}{1+e^{-(V+14.1)/6.0}}\right)(V - E_{\mathrm{Ca,L}})(1-b)$$

$$\frac{\mathrm{d}d_{\mathrm{L}}}{\mathrm{d}t} = \frac{d_{\mathrm{L}\infty} - d_{\mathrm{L}}}{\tau_{d_{\mathrm{L}}}}$$

$$d_{\mathrm{L}\infty} = \frac{1.0}{1 + e^{-(V+23.1)/6.0}}, \quad \tau_{d_{\mathrm{L}}} = \frac{1000.0}{\alpha_{d_{\mathrm{L}}} + \beta_{d_{\mathrm{L}}}}$$

$$\alpha_{d_{\mathrm{L}}} = -\frac{14.19(V+35.0)}{e^{-(V+14.1)/2.5} - 1} - \frac{42.45V}{e^{-0.208V} - 1}, \quad \beta_{d_{\mathrm{L}}} = \frac{5.71(V-5.0)}{e^{(V-5.0)/2.5} - 1}$$

$$\frac{\mathrm{d}f_{\mathrm{L}}}{\mathrm{d}t} = \frac{f_{\mathrm{L}\infty} - f_{\mathrm{L}}}{\tau_{f_{\mathrm{L}}}}$$

$$f_{\mathrm{L}\infty} = \frac{\alpha_{f_{\mathrm{L}}}}{\alpha_{f_{\mathrm{L}}} + \beta_{f_{\mathrm{L}}}}, \quad \tau_{f_{\mathrm{L}}} = \frac{1000.0}{\alpha_{f_{\mathrm{L}}} + \beta_{f_{\mathrm{L}}}}$$

$$\alpha_{f_{\mathrm{L}}} = \frac{3.12(V+28.0)}{e^{(V+28.0)/4.0} - 1}, \quad \beta_{f_{\mathrm{L}}} = \frac{25.0}{1 + e^{-(V+28.0)/4.0}}$$

$$b = b_{\max} \frac{[\mathrm{ACh}]}{K_{0.5,Ca} + [\mathrm{ACh}]}$$

Model II.3. T-type Ca^{2+} current

$$I_{\mathrm{Ca,\,T}} = g_{\mathrm{Ca,\,T}} d_{\mathrm{T}} f_{\mathrm{T}} (V - E_{\mathrm{Ca,\,T}})$$

$$\frac{\mathrm{d}d_{\mathrm{T}}}{\mathrm{d}t} = \frac{d_{\mathrm{T}\infty} - d_{\mathrm{T}}}{\tau_{d_{\mathrm{T}}}}$$

$$d_{\mathrm{T}\infty} = \frac{1.0}{1 + e^{-(V+37.0)/6.8}}, \quad \tau_{d_{\mathrm{T}}} = \frac{1000.0}{\alpha_{d_{\mathrm{T}}} + \beta_{d_{\mathrm{T}}}}$$

$$\alpha_{d_{\mathrm{T}}} = 1068\, e^{(V+26.3)/30.0}, \quad \beta_{d_{\mathrm{T}}} = 1068\, e^{-(V+26.3)/30.0}$$

$$\frac{\mathrm{d}f_{\mathrm{T}}}{\mathrm{d}t} = \frac{f_{\mathrm{T}\infty} - f_{\mathrm{T}}}{\tau_{f_{\mathrm{T}}}}$$

$$f_{\mathrm{T}\infty} = \frac{1.0}{1 + e^{(V+71)/9}}, \quad \tau_{f_{\mathrm{T}}} = \frac{1000.0}{\alpha_{f_{\mathrm{T}}} + \beta_{f_{\mathrm{T}}}}$$

$$\alpha_{f_{\mathrm{T}}} = 15.3 e^{-(V+71.7)/83.33}, \quad \beta_{f_{\mathrm{T}}} = 15^{(V+71.7)/15.38}$$

Model II.4. Transient outward K^+ current

$$I_{\mathrm{to}} = g_{\mathrm{to}} qr(V - E_{\mathrm{K}})$$

$$\frac{\mathrm{d}r}{\mathrm{d}t} = \frac{r_{\infty} - r}{\tau_r}$$

$$r_{\infty} = \frac{1.0}{1 + e^{-(V-10.93)/19.7}}, \quad \tau_r = 1000 \left(2.98 \times 10^{-3} + \frac{15.59 \times 10^{-3}}{1.037\mathrm{e}^{\,0.09\,(\mathrm{V}+30.61)} + 0.369\, e^{-0.12\,(V+23.84)}} \right)$$

$$\frac{\mathrm{d}q}{\mathrm{d}t} = \frac{q_{\infty} - q}{\tau_{q_1}}$$

$$q_\infty = \frac{1.0}{1+e^{(V+59.37)/13.1}},$$

$$\tau_q = 1000\left(10.1\times10^{-3} + \frac{65.17\times10^{-3}}{0.57\,e^{-0.08\,(V+498)}} + 0.24\times10^{-4}\,e^{0.1(V+50.93)}\right)$$

Model II.5. Sustained outward current

$$I_{\text{sus}} = g_{\text{sus}}\,(V - E_{\text{sus}})$$

Model II.6. Fast delayed rectifier K^+ current

$$I_{\text{K,r}} = g_{\text{K,r}}\,p_a\,p_i(V - E_K)$$

$$p_a = (1 - F_{K,r})\,p_{a,f} + F_{K,r}\,p_{a,s}$$

$$\frac{\mathrm{d}p_{a,f}}{\mathrm{d}t} = \frac{p_{a\infty} - p_{a,f}}{\tau_{p_a,f}}, \quad \frac{\mathrm{d}p_{a,s}}{\mathrm{d}t} = \frac{p_{a\infty} - p_{a,s}}{\tau_{p_a,s}}$$

$$p_{a\infty} = \frac{1.0}{1+e^{-(V+14.2)/10.6}}$$

$$\tau_{p_a,f} = 1000\left(\frac{1.0}{37.2\mathrm{e}^{(\mathrm{V}-9)/15.9} + 0.96e^{-(V-9)/22.5}}\right), \tau_{p_a,s} = 1000\left(\frac{1.0}{4.2\mathrm{e}^{(\mathrm{V}-9)/15.9} + 0.15e^{-(V-9)/21.6}}\right)$$

$$\frac{\mathrm{d}p_i}{\mathrm{d}t} = \frac{p_{i\infty} - p_i}{\tau_{p_i}}$$

$$p_{i\infty} = \frac{1.0}{1+e^{(V+18.6)/10.1}}, \quad \tau_{p_i} = 2.0$$

Model II.7. Slow delayed rectifier K^+ current

$$I_{\text{K,s}} = g_{\text{K,s}}\,x_s^2(V - E_K)$$

$$\frac{\mathrm{d}x_s}{\mathrm{d}t} = \frac{x_{s\infty} - x_s}{\tau_{x_s}}$$

$$x_{s\infty} = \frac{\alpha_{x_s}}{\alpha_{x_s} + \beta_{x_s}}, \quad \tau_{x_s} = \frac{1000.0}{\alpha_{x_s} + \beta_{x_s}}$$

$$\alpha_{x_s} = \frac{14.0}{1+e^{-(V-40)/9}}, \quad \beta_{x_s} = e^{-V/45}$$

Model II.8. "Funny" current

$$I_f = I_{f,Na} + I_{f,K}$$

$$I_{f,Na} = g_{\text{f,Na}}\,y(V - E_{Na})$$

$$I_{f,K} = g_{\text{f,K}}\,y(V - E_K)$$

$$\frac{\mathrm{d}y}{\mathrm{d}t} = \frac{y_\infty - y}{\tau_y}$$

$$y_\infty = \frac{\alpha_y}{\alpha_y + \beta_y}, \quad \tau_y = \frac{1000.0}{\alpha_y + \beta_y}$$

$$\alpha_y = e^{-(V+78.91-s)/26.2}, \quad \beta_y = e^{(V+75.131-s)/21.25}$$

$$s = s_{\max} \frac{[\mathrm{ACh}]^{nf}}{K_{0.5,f}^{nf} + [\mathrm{ACh}]^{nf}}$$

Model II.9. Na^+-Ca^{2+} exchanger current

$$I_{\mathrm{NaCa}} = k_{\mathrm{NaCa}} \frac{[\mathrm{Na}^+]_\mathrm{i}^3 [\mathrm{Ca}^{2+}]_\mathrm{o} e^{\gamma_{\mathrm{NaCa}} VF/RT} - [\mathrm{Na}^+]_\mathrm{o}^3 [\mathrm{Ca}^{2+}]_\mathrm{i} e^{(\gamma_{\mathrm{NaCa}}-1)VF/RT}}{1 + d_{\mathrm{NaCa}}([\mathrm{Na}^+]_\mathrm{i}^3 [\mathrm{Ca}^{2+}]_\mathrm{o} + [\mathrm{Na}^+]_\mathrm{o}^3 [\mathrm{Ca}^{2+}]_\mathrm{i})}$$

Model II.10. Na^+-K^+ pump current

$$I_{\mathrm{NaK}} = \bar{I}_{\mathrm{NaK}} \left(\frac{[\mathrm{Na}^+]_\mathrm{i}}{K_{\mathrm{m,Na}} + [\mathrm{Na}^+]_\mathrm{i}} \right)^3 \left(\frac{[\mathrm{K}^+]_\mathrm{o}}{K_{\mathrm{m,K}} + [\mathrm{K}^+]_\mathrm{o}} \right)^2 \frac{1.6}{1.5 + e^{-(V+60)/40}}$$

Model II.11. Background currents

$$I_{\mathrm{Na,b}} = g_{\mathrm{Na,b}}(V - E_{\mathrm{Na}}), \quad I_{\mathrm{Ca,b}} = g_{\mathrm{Ca,b}}(V - E_{\mathrm{Ca}}), \; I_{\mathrm{K,b}} = g_{\mathrm{K,b}}(V - E_K)$$

Model II.12. Acetylcholine activated K^+ current

$$I_{\mathrm{K,ACh}} = g_{\mathrm{K,ACh}} \left(\frac{[K]_e}{10 + [K]_e} \right) \frac{(V - E_K)}{1 + e^{(V - E_K - 140)F/2.5RT}}$$

$$g_{\mathrm{K,ACh}} = \bar{g}_{\mathrm{K,ACh}} jk \frac{[\mathrm{ACh}]^{nk,ACh}}{K_{0.5,K,ACh}^{nk,ACh} + [\mathrm{ACh}]^{nk,ACh}}$$

$$\frac{\mathrm{d}j}{\mathrm{d}t} = \frac{j_\infty - j}{\tau_j}$$

$$j_\infty = \frac{\alpha_j}{\alpha_j + \beta_j}, \; \tau_j = \frac{1000.0}{\alpha_j + \beta_j}$$

$$\alpha_j = 73.1, \quad \beta_j = \frac{120}{1 + e^{-(V+50)/15}}$$

$$\frac{\mathrm{d}k}{\mathrm{d}t} = \frac{k_\infty - k}{\tau_k}$$

$$k_\infty = \frac{\alpha_k}{\alpha_k + \beta_k}, \; \tau_k = \frac{1000.0}{\alpha_k + \beta_k}$$

$$\alpha_k = 3.7, \quad \beta_k = \frac{5.82}{1 + e^{-(V+50)/15}}$$

Online Table II. Model parameter values

	Center	Periphery
$B_{\max}$	0.56	0.56
C_m	20 pF	65 pF
D_{NaCa}	0.0001	0.0001
$E_{\mathrm{Ca,L}}$	46.4 mV	46.4 mV

$E_{Ca,T}$	45 mV	45 mV
E_{sus}	-	-
G_{Na}	0 μS/pF	1.85×10^{-8} μS/pF
$G_{Ca,L}$	2.9×10^{-4} μS/pF	1.0×10^{-3} μS/pF
$G_{Ca,T}$	2.14×10^{-4} μS/pF	2.14×10^{-4} μS/pF
G_{to}	2.5×10^{-4} μS/pF	5.6×10^{-4} μS/pF
G_{sus}	3.3×10^{-6} μS/pF	1.8×10^{-4} μS/pF
$G_{K,ACh}$	3.53×10^{-10} μS/pF	1.218×10^{-9} μS/pF
$G_{K,r}$	3.99×10^{-5} μS/pF	2.46×10^{-4} μS/pF
$G_{K,s}$	2.59×10^{-5} μS/pF	1.6×10^{-4} μS/pF
G_{K1}	-	-
$G_{f,Na}$	0.27×10^{-4} μS/pF	1.05×10^{-4} μS/pF
$G_{f,K}$	0.27×10^{-4} μS/pF	1.05×10^{-4} μS/pF
$G_{b,Na}$	2.91×10^{-6} μS/pF	2.9×10^{-6} μS/pF
$G_{b,Ca}$	6.62×10^{-7} μS/pF	6.61×10^{-7} μS/pF
$G_{b,K}$	1.3×10^{-6} μS/pF	1.3×10^{-6} μS/pF
$\bar{I}_{NaK}$	2.46×10^{-3} nA/pF	2.46×10^{-3} nA/pF
K_{NaCa}	1.36×10^{-7} μS/pF	1.36×10^{-7} μS/pF
$[Na^+]_o$	140 mM	140 mM
$[Na^+]_i$	8 mM	8 mM
$[Ca^{2+}]_o$	2 mM	2 mM
$[Ca^{2+}]_i$	0.0001 mM	0.0001 mM
$[K^+]_o$	5.4 mM	5.4 mM
$[K^+]_i$	140 mM	140 mM
$K_{m,K}$	0.621	0.621
$K_{m,Na}$	5.64	5.64
$K_{0.5,Ca}$	0.09 μM	0.09 μM
$K_{0.5,f}$	1.26×10^{-2} μM	1.26×10^{-2} μM
$K_{0.5,K,ACh}$	0.28 μM	0.28 μM
$N_{K,ACh}$	1.5	1.5
N_f	0.69	0.69
S_{max}	-7.2 mV	-7.2 mV
Γ_{NaCa}	0.5	0.5

Model III. Atrial cell model

$$I_{\text{tot}} = I_{\text{Na}} + I_{\text{Ca,L}} + I_{\text{Ca,T}} + I_{\text{to}} + I_{\text{sus}} + I_{\text{K,r}} + I_{\text{K,s}} + I_{\text{K1}} + I_{\text{NaCa}} + I_{\text{NaK}} + I_{\text{Na,b}} + I_{\text{Ca,b}} + I_{\text{Ca,p}}$$

Model III.1. Fast Na^+ current

$$I_{\text{Na}} = g_{\text{Na}} m^3 h [\text{Na}^+]_{\text{o}} \frac{VF^2}{RT} \frac{e^{(V-E_{\text{Na}})F/RT} - 1}{e^{VF/RT} - 1}$$

$$\frac{\text{d}m}{\text{d}t} = \frac{m_\infty - m}{\tau_m}$$

$$m_\infty = \frac{\alpha_m}{\alpha_m + \beta_m}, \quad \tau_m = \frac{1000.0}{\alpha_m + \beta_m}$$

$$\alpha_m = \frac{460.0(V + 44.4)}{1 - e^{-(V+44.4)/12.673}}, \quad \beta_m = 18400\ .0 e^{-(V+44.4)/12.673}$$

$$h = 0.635\, h_1 + 0.365\, h_2$$

$$\frac{\text{d}h_1}{\text{d}t} = \frac{h_{1\infty} - h_1}{\tau_{h_1}}, \quad \frac{\text{d}h_2}{\text{d}t} = \frac{h_{2\infty} - h_2}{\tau_{h_2}}$$

$$h_{1\infty} = h_{2\infty} = \frac{\alpha_h}{\alpha_h + \beta_h}$$

$$\alpha_h = 44.9 e^{-(V+66.9)/5.57}, \quad \beta_h = \frac{1491.0}{1 + 323.3 e^{-(V+94.6)/12.9}}$$

$$\tau_{h_1} = 1000\left(\frac{0.03}{1 + e^{(V+40.0)/6.0}} + 0.00015 \right)$$

$$\tau_{h_2} = 1000\left(\frac{0.12}{1 + e^{(V+55.0)/2.0}} + 0.00045 \right)$$

Model III.2. L-type Ca^{2+} current

$$I_{\text{Ca,L}} = g_{\text{Ca,L}}\left(d_{\text{L}} f_{\text{L}} + \frac{1.0}{1 + e^{-(V-23)/12.0}} \right)(V - E_{\text{Ca,L}})$$

$$\frac{\text{d}d_{\text{L}}}{\text{d}t} = \frac{d_{\text{L}\infty} - d_{\text{L}}}{\tau_{d_{\text{L}}}}$$

$$d_{\text{L}\infty} = \frac{1.0}{1 + e^{-(V+10.95)/6.6}}, \quad \tau_{d_{\text{L}}} = \frac{1000.0}{\alpha_{d_{\text{L}}} + \beta_{d_{\text{L}}}}$$

$$\alpha_{d_{\text{L}}} = \frac{16.72(V + 45.0)}{1 - e^{-(V+45.0)/2.5}} + \frac{50.0(V + 10)}{1 - e^{-(V+10)/4.808}}, \quad \beta_{d_{\text{L}}} = \frac{4.48(V + 5.0)}{e^{(V+5.0)/2.5} - 1}$$

$$\frac{\text{d}f_{\text{L}}}{\text{d}t} = \frac{f_{\text{L}\infty} - f_{\text{L}}}{\tau_{f_{\text{L}}}}$$

$$f_{\text{L}\infty} = \frac{\alpha_{f_{\text{L}}}}{\alpha_{f_{\text{L}}} + \beta_{f_{\text{L}}}}, \quad \tau_{f_{\text{L}}} = \frac{1000.0}{\alpha_{f_{\text{L}}} + \beta_{f_{\text{L}}}}$$

$$\alpha_{f_{\text{L}}} = \frac{8.49(V + 18.0)}{e^{(V+18.0)/4.0} - 1}, \quad \beta_{f_{\text{L}}} = \frac{67.922}{1 + e^{-(V+18.0)/4.0}}$$

Model III.3. T-type Ca^{2+} current

$$I_{\text{Ca,T}} = g_{\text{Ca,T}} d_T f_T (V - E_{\text{Ca,T}})$$

$$\frac{\mathrm{d}d_{\mathrm{T}}}{\mathrm{d}t} = \frac{d_{\mathrm{T}\infty} - d_{\mathrm{T}}}{\tau_{d_{\mathrm{T}}}}$$

$$d_{\mathrm{T}\infty} = \frac{1.0}{1 + e^{-(V+23.0)/6.1}}, \quad \tau_{d_{\mathrm{T}}} = \frac{1000.0}{\alpha_{d_{\mathrm{T}}} + \beta_{d_{\mathrm{T}}}}$$

$$\alpha_{d_{\mathrm{T}}} = 674.173 e^{-(V+23.0)/30.0}, \quad \beta_{d_{\mathrm{T}}} = 674.173 e^{(V+23.0)/30.0}$$

$$\frac{\mathrm{d}f_{\mathrm{T}}}{\mathrm{d}t} = \frac{f_{\mathrm{T}\infty} - f_{\mathrm{T}}}{\tau_{f_{\mathrm{T}}}}$$

$$f_{\mathrm{T}\infty} = \frac{\alpha_{f_{\mathrm{T}}}}{\alpha_{f_{\mathrm{T}}} + \beta_{f_{\mathrm{T}}}}, \quad \tau_{f_{\mathrm{T}}} = \frac{1000.0}{\alpha_{f_{\mathrm{T}}} + \beta_{f_{\mathrm{T}}}}$$

$$\alpha_{f_{\mathrm{T}}} = 9.637 e^{-(V+75.0)/83.33}, \quad \beta_{f_{\mathrm{T}}} = 9.637 e^{(V+75.0)/15.38}$$

Model III.4. Transient outward K^+ current

$$I_{\mathrm{to}} = g_{\mathrm{to}} r \left(0.59 s_1^3 + 0.41 s_2^3\right)\left(0.6 s_3^6 + 0.4\right)\left(V - E_{\mathrm{K}}\right)$$

$$\frac{\mathrm{d}r}{\mathrm{d}t} = \frac{r_\infty - r}{\tau_r}$$

$$r_\infty = \frac{1.0}{1 + e^{-(V+15.0)/5.633}}, \quad \tau_r = 1000\left(\frac{1.0}{\alpha_r + \beta_r} + 0.0004\right)$$

$$\alpha_r = 386.6 e^{V/12.0}, \quad \beta_r = 8.011 e^{-V/7.2}$$

$$\frac{\mathrm{d}s_1}{\mathrm{d}t} = \frac{s_{1\infty} - s_1}{\tau_{s_1}}, \quad \frac{\mathrm{d}s_2}{\mathrm{d}t} = \frac{s_{2\infty} - s_2}{\tau_{s_2}}$$

$$s_{1\infty} = s_{2\infty} = \frac{1.0}{1 + e^{(V+28.29)/7.06}}$$

$$\tau_{s_1} = 1000\left(\frac{0.189}{1 + e^{(V+32.8)/0.1}} + 0.0204\right)$$

$$\tau_{s_2} = 1000\left(\frac{0.189}{1 + e^{(V+32.8)/0.1}} + 0.45 e^{-(V-13.54)/13.97}\right)$$

$$\frac{\mathrm{d}s_3}{\mathrm{d}t} = \frac{s_{3\infty} - s_3}{\tau_{s_3}}$$

$$s_{3\infty} = \left[\frac{1.0}{1 + e^{(V+50.67)/27.38}} + 0.666\right]/1.666$$

$$\tau_{s_3} = 1000\left(\frac{7.5}{1 + e^{(V+23.0)/0.5}} + 0.5\right)$$

Model III.5. Sustained outward current

$$I_{\mathrm{sus}} = g_{\mathrm{sus}} (V - E_{\mathrm{sus}})$$

Model III.6. Fast delayed rectifier K^+ current

$$I_{\mathrm{K,r}} = g_{\mathrm{K,r}} p_a p_i (V - E_K)$$

$$\frac{\mathrm{d}p_a}{\mathrm{d}t} = \frac{p_{a\infty} - p_a}{\tau_{p_a}}$$

$$p_{a\infty} = \frac{1.0}{1+e^{-(V+5.1)/7.4}}, \quad \tau_{p_a} = \frac{1000.0}{\alpha_{p_a}+\beta_{p_a}}$$

$$\alpha_{p_a} = 9.0e^{-V/25.371}, \quad \beta_{p_a} = 1.3e^{-V/13.026}$$

$$\frac{\mathrm{d}p_i}{\mathrm{d}t} = \frac{p_{i\infty}-p_i}{\tau_{p_i}}$$

$$p_{i\infty} = \frac{\alpha_{p_i}}{\alpha_{p_i}+\beta_{p_i}}, \quad \tau_{p_i} = \frac{1000.0}{\alpha_{p_i}+\beta_{p_i}}$$

$$\alpha_{p_i} = 100.0e^{-V/54.645}, \quad \beta_{p_i} = 656.0e^{V/106.157}$$

Model III.7. Slow delayed rectifier K^+ current

$$I_{\mathrm{K,s}} = g_{\mathrm{K,s}} n(V - E_K)$$

$$\frac{\mathrm{d}n}{\mathrm{d}t} = \frac{n_\infty - n}{\tau_n}$$

$$n_\infty = \frac{1.0}{1+e^{-(V+0.9)/13.8}}, \quad \tau_n = 1000\left(\frac{1.0}{\alpha_n+\beta_n}+0.060\right)$$

$$\alpha_n = 1.66\,e^{V/69.452}, \quad \beta_n = 0.3e^{-V/21.826}$$

Model III.8. Inward rectifier K^+ current

$$I_{\mathrm{K1}} = g_{\mathrm{K1}}\left(\frac{[\mathrm{K}^+]_\mathrm{o}}{K_{\mathrm{m,K1}}+[\mathrm{K}^+]_\mathrm{o}}\right)^3 \frac{V-E_\mathrm{K}}{1+e^{1.393(V-E_\mathrm{K}+3.6)F/RT}}$$

Model III.9. Na^+-Ca^{2+} exchanger current

$$I_{\mathrm{NaCa}} = k_{\mathrm{NaCa}} \frac{[\mathrm{Na}^+]_\mathrm{i}^3[\mathrm{Ca}^{2+}]_\mathrm{o} e^{\gamma_{\mathrm{NaCa}}VF/RT} - [\mathrm{Na}^+]_\mathrm{o}^3[\mathrm{Ca}^{2+}]_\mathrm{i} e^{(\gamma_{\mathrm{NaCa}}-1)VF/RT}}{1+d_{\mathrm{NaCa}}([\mathrm{Na}^+]_\mathrm{i}^3[\mathrm{Ca}^{2+}]_\mathrm{o}+[\mathrm{Na}^+]_\mathrm{o}^3[\mathrm{Ca}^{2+}]_\mathrm{i})}$$

Model III.10. Na^+-K^+ pump current

$$I_{\mathrm{NaK}} = \bar{I}_{\mathrm{NaK}}\left(\frac{[\mathrm{Na}^+]_\mathrm{i}^{1.5}}{K_{\mathrm{m,Na}}^{1.5}+[\mathrm{Na}^+]_\mathrm{i}^{1.5}}\right)\left(\frac{[\mathrm{K}^+]_\mathrm{o}}{K_{\mathrm{m,K}}+[\mathrm{K}^+]_\mathrm{o}}\right)\frac{1.6}{1.5+e^{-(V+60)/40}}$$

Model III.11. Ca^{2+} pump current

$$I_{\mathrm{Ca,p}} = \bar{I}_{\mathrm{Ca,p}} \frac{[\mathrm{Ca}^{2+}]_\mathrm{i}}{[\mathrm{Ca}^{2+}]_\mathrm{i}+0.0002}$$

Model III.12. Background currents

$$I_{\mathrm{Na,b}} = g_{\mathrm{Na,b}}(V-E_{\mathrm{Na}}), \quad I_{\mathrm{Ca,b}} = g_{\mathrm{Ca,b}}(V-E_{\mathrm{Ca}})$$

Online Table III. Model parameter values

g_{Na}	0.028×10^{-6} μS/pF
$g_{Ca,L}$	144.0×10^{-6} μS/pF
$g_{Ca,T}$	120.0×10^{-6} μS/pF
g_{to}	200.0×10^{-6} μS/pF
g_{sus}	26.00×10^{-6} μS/pF
$g_{K,r}$	70.00×10^{-6} μS/pF
$g_{K,s}$	50.00×10^{-6} μS/pF
g_{K1}	203.2×10^{-6} μS/pF
$g_{Na,b}$	0.400×10^{-6} μS/pF
$g_{Ca,b}$	0.400×10^{-6} μS/pF
k_{NaCa}	0.400×10^{-6} μS/pF
I_{NaK}	1.288×10^{-3} nA/pF
$I_{Ca,p}$	190.0×10^{-6} μS/pF
d_{NaCa}	0.0003
γ_{NaCa}	0.4500
$K_{m,Na}$	11.00 mM
$K_{m,K}$	1.000 mM
$K_{m,K1}$	0.590 mM
$[Na^+]_o$	140.0 mM
$[Ca^{2+}]_o$	2.500 mM
$[K^+]_o$	5.000 mM
E_{sus}	-70 mV
$E_{Ca,L}$	50 mV
$E_{Ca,T}$	38 mV
R	8314 mJ/mol °C
F	96487 C/mol
T	35°C

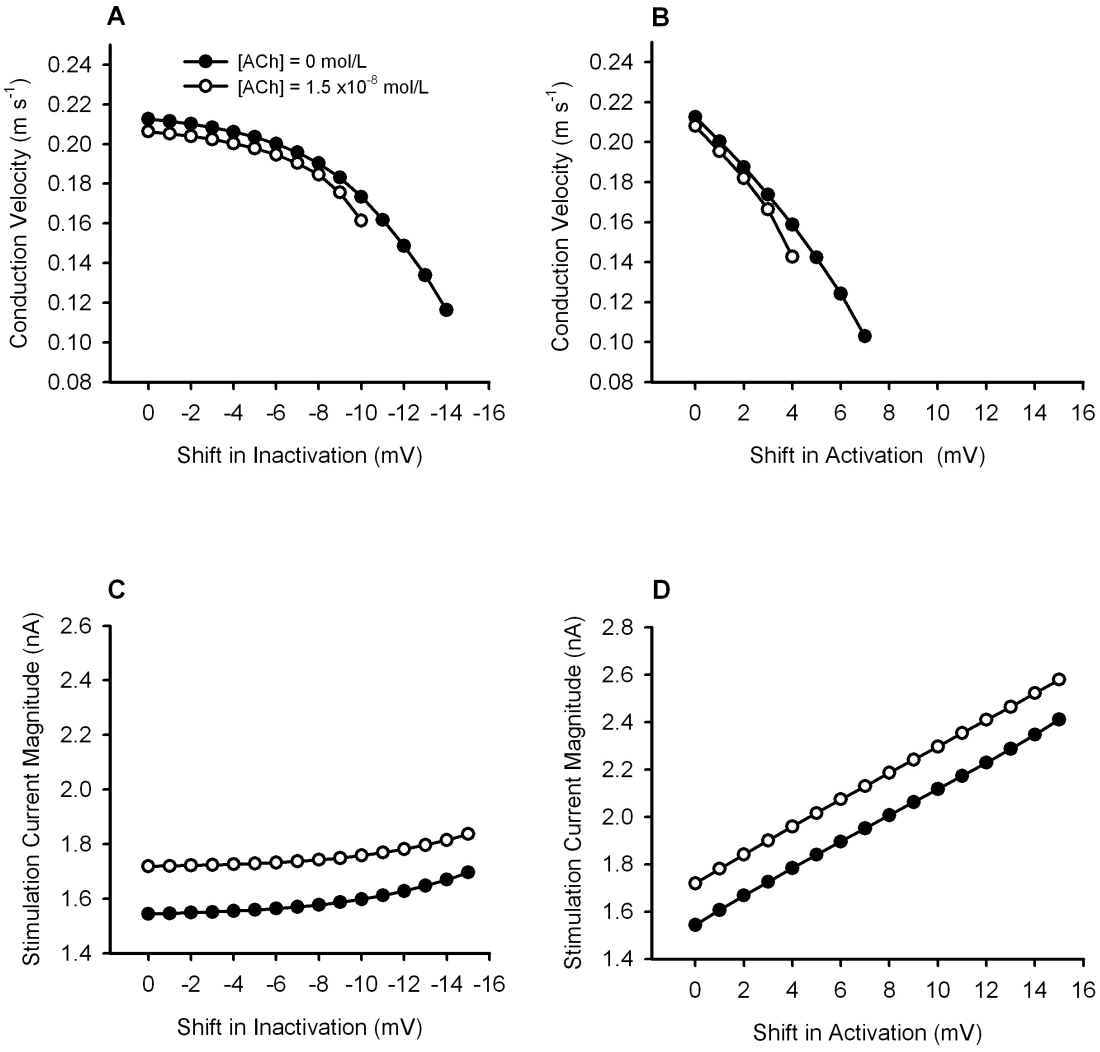

Online Figure I. Effects of shifts in steady-state voltage-dependent inactivation/activation associated with G1/G2 mutations on atrial excitability. A, B: Conduction velocity in one-dimensional atrial tissue against a shift of the steady-state inactivation (A) or activation (B) curve. C, D: Excitation threshold of a single atrial cell against a shift of the steady-state inactivation (C) or activation (D) curve. [ACh] = 0 (closed circles) or [ACh] = 1.5 $\times 10^{-8}$ mol/L (open circles).

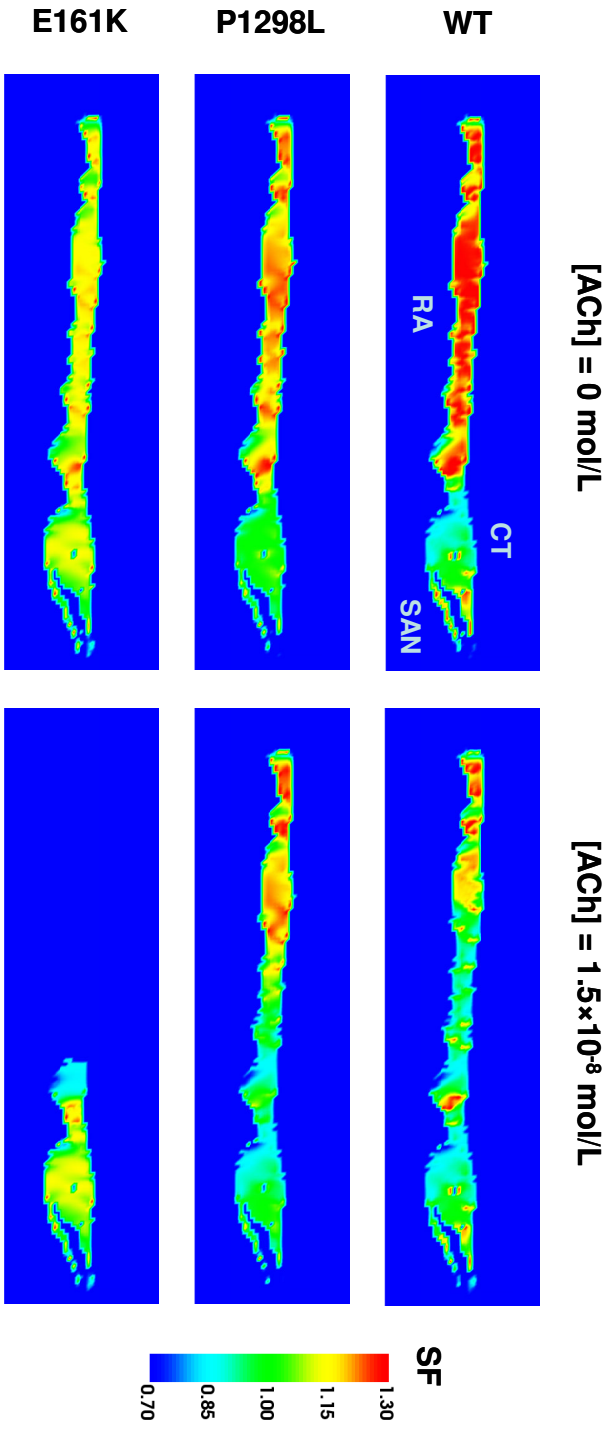

Online Figure II. Effects of the SCN5A mutations and ACh on the AP conduction safety. Spatial distributions of the SF during AP conduction from the SAN into the RA in the 2D tissue slice model are colour-coded according to palette on the right; mutations (P1298L and E161K) and ACh concentrations are indicated in the respective labels.